

Analysis of Static Deformation, Vibration and Active Damping of Cylindrical Composite Shells with Piezoelectric Shear Actuators

Senthil S. Vel

Assistant Professor
Department of Mechanical Engineering

Brian P. Baillargeon

Graduate Student
Department of Mechanical Engineering,
University of Maine, Orono, Maine 04469

An analytical solution is presented for the static deformation and steady-state vibration of simply supported hybrid cylindrical shells consisting of fiber-reinforced layers with embedded piezoelectric shear sensors and actuators. The piezoelectric shear actuator, which is poled in the circumferential direction, will induce transverse shear deformation of the hybrid shell when it is subjected to an electric field in the radial direction. Suitable displacement and electric potential functions that identically satisfy the boundary conditions at the simply supported edges are used to reduce the governing equations of static deformation and steady-state vibrations of the hybrid laminate to a set of coupled ordinary differential equations in the radial coordinate, which are solved by employing the Frobenius method. Natural frequencies, mode shapes, displacements, electric potential, and stresses are presented for four-layer hybrid laminates consisting of a piezoelectric shear sensor and actuator sandwiched between fiber-reinforced composite layers. Active vibration damping is implemented using a positive position feedback controller. Frequency response curves for different controller frequencies, controller damping ratio, and feedback gain demonstrate that the embedded shear actuator can be used for active damping of the fundamental flexural mode. In addition, it is demonstrated that vibration suppression of thickness modes is also feasible using the piezoelectric shear actuator. [DOI: 10.1115/1.1898337]

1 Introduction

A class of smart/adaptive structures, consisting of piezoelectric materials integrated with structural systems, has found widespread use in engineering applications. Numerous applications have been proposed and conceived experimentally, such as for active vibration suppression [1–3] and noise cancellation [4]. A piezoelectric actuator in an adaptive structure is a thin rectangular element that is generally poled in the thickness direction and is usually bonded to the surfaces of the host structure. The application of an electric field in the thickness direction causes the actuator's lateral dimensions to increase or decrease. The lateral deformations of the actuator force the host structure to deform. In order to successfully incorporate piezoelectric actuators into a structure, the mechanical interaction between the actuators and the host structure must be fully understood. Several analytical and finite element studies have been presented for hybrid beams and plates with thickness-poled actuators [5–9]. Chen et al. [10], Dumir et al. [11], and Chen and Shen [12] have presented analytical solutions for the plane strain static deformation and free vibration of hybrid composite shells with radially poled piezoelectric actuators.

Piezoelectric actuators poled in the thickness direction are usually placed at the extreme thickness positions of a plate-like structure to achieve the most effective actuation. This subjects the actuators to high longitudinal stresses that may be detrimental to the brittle piezoceramic material. Furthermore, surface-bonded actuators are likely to be damaged by contact with surrounding objects. To alleviate these problems Sun and Zhang [13] proposed an adaptive sandwich structure consisting of an axially poled piezoelectric core sandwiched between two elastic facing sheets. The application of an electric field in the thickness direction will induce transverse shear deformation of the core, thus generating the

desired transverse deflection of the sandwich structure. Piezoelectric actuators poled in such a way as to produce transverse shear deformation under the action of an electric field in the thickness direction are called *shear actuators*. Piezoelectric shear actuators of various dimensions are commercially available [14]. Zhang and Sun [15,16] developed a beam theory for sandwich structures containing shear actuators by modeling the facing sheets as classical Euler–Bernoulli beams and the central core as a Timoshenko beam which allows transverse shear deformation. Benjeddou et al. [17] developed a unified finite element model for extension and shear actuation mechanisms with more detailed formulation of the electric problem. Theoretical and finite element models for the vibration control of sandwich beams with shear actuators have demonstrated that shear actuators can be more effective than thickness-poled actuators for the control of bending vibrations [18]. Benjeddou and Deü [19] have analyzed the vibration of a piezoelectric sandwich plate using a layer-wise first-order shear deformation theory and through-thickness quadratic electric profile. Vel and Batra [20,21] gave an analytical solution for the static bending of a simply supported sandwich plate with an embedded piezoelectric shear actuator. Benjeddou et al. [22,23] presented a theoretical formulation based on the first-order shear deformation theory and finite element implementation for shells of revolution that consist of a piezoelectric shear core embedded within elastic facings. Recently, Baillargeon and Vel [24] obtained an analytical solution for the free vibration, forced vibration, and active vibration suppression of hybrid plates with an embedded shear actuator.

The analytical solution procedure for the bending and vibration of composite shells with radially poled piezoelectric actuators given by Chen et al. [10], Dumir et al. [11], and Chen and Shen [12] are not applicable when the piezoelectric layers are poled in the circumferential direction. Here we derive an analytical solution for the static deformation and steady-state vibration of composite shells with embedded piezoelectric shear actuators and sensors. The equations of motion, charge equation and constitutive equations of linear piezoelectricity are exactly satisfied at every

Contributed by the Technical Committee on Vibration and Sound for publication in the JOURNAL OF VIBRATION AND ACOUSTICS. Manuscript received August 26, 2003; Final Manuscript received August 5, 2004. Review conducted by: John A. Main.

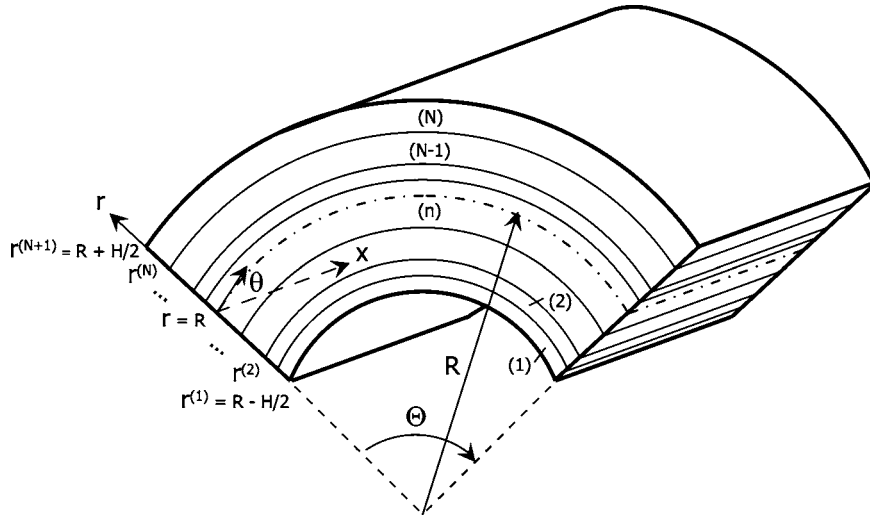


Fig. 1 *N*-layer hybrid piezoelectric shell

point in the hybrid shell. The boundary conditions at the simply supported edges, the traction boundary conditions on the inner and outer surfaces of the shell and the electromechanical continuity conditions at the interfaces between dissimilar layers are also exactly satisfied. The first nine natural frequencies, mode shapes, and through-the-thickness plots of the displacements and stresses are presented for sandwich shells consisting of circumferentially poled piezoelectric sensor and actuator that are sandwiched between two fiber-reinforced composite layers. The analytical and finite element results are in good agreement for the static deformation and natural frequencies. Active vibration damping is implemented using a positive position feedback controller [25–27] wherein a second-order compensator is forced by the electric potential of the sensor. The controller coordinate, amplified by a gain, is then fed back as a voltage input to the piezoelectric shear actuator. Frequency response curves for several different controller frequencies, controller damping ratio, and feedback gain demonstrate that the embedded shear actuator can be used for active damping of the fundamental flexural mode. In addition, vibration suppression of the thickness modes can also be achieved using the shear actuator.

2 Formulation of the Problem

A cylindrical polar coordinate system, shown in Fig. 1, is used to describe the infinitesimal deformations of an *N*-layer hybrid cylindrical shell. The shell is of extent Θ in the θ direction, H in the r direction, and infinitely long in the x direction. The variable R denotes the radial location of the mid-surface of the shell. The radial locations of the bottom surface, $N-1$ interfaces between adjoining laminae and the top surface of the shell are denoted by $r^{(1)}=R-H/2$, $r^{(2)}, \dots, r^{(n)}, \dots, r^{(N)}, r^{(N+1)}=R+H/2$. Each lamina is assumed to be made of a homogeneous material.

The equations of motion for lamina n , in the absence of body forces and free charges, are

$$\begin{aligned} \sigma_{rr,r}^{(n)} + \frac{1}{r} \sigma_{r\theta,\theta}^{(n)} + \sigma_{xr,x}^{(n)} + \frac{1}{r} (\sigma_{rr}^{(n)} - \sigma_{\theta\theta}^{(n)}) &= \rho^{(n)} \ddot{u}_r^{(n)}, \\ \sigma_{r\theta,r}^{(n)} + \frac{1}{r} \sigma_{\theta\theta,\theta}^{(n)} + \sigma_{x\theta,x}^{(n)} + \frac{2}{r} \sigma_{r\theta}^{(n)} &= \rho^{(n)} \ddot{u}_\theta^{(n)}, \\ \sigma_{rx,r}^{(n)} + \frac{1}{r} \sigma_{\theta x,\theta}^{(n)} + \sigma_{xx,x}^{(n)} + \frac{1}{r} \sigma_{rx}^{(n)} &= \rho^{(n)} \ddot{u}_x^{(n)}, \end{aligned} \quad (1)$$

$$D_{r,r}^{(n)} + \frac{1}{r} (D_{\theta,\theta}^{(n)} + D_r^{(n)}) + D_{x,x}^{(n)} = 0.$$

where σ , u , and D denote the Cauchy stress tensor, displacement vector, and electric displacement vector, respectively, ρ is the mass density and differentiation is indicated by a subscript comma. A superimposed dot denotes differentiation with respect to time t and the superscript (n) signifies quantities for lamina n .

The fiber-reinforced elastic layers are orthotropic with principle material direction oriented at an angle to the θ axis in the θ - x surface. The piezoelectric layers are transversely isotropic and poled in the θ direction. The constitutive equations, in contracted notation, for lamina n are

$$\begin{Bmatrix} \sigma_{\theta\theta} \\ \sigma_{xx} \\ \sigma_{rr} \\ \sigma_{xr} \\ \sigma_{r\theta} \\ \sigma_{\theta x} \end{Bmatrix}^{(n)} = \begin{bmatrix} C_{11} & C_{12} & C_{13} & 0 & 0 & C_{16} \\ C_{12} & C_{22} & C_{23} & 0 & 0 & C_{26} \\ C_{13} & C_{23} & C_{33} & 0 & 0 & C_{36} \\ 0 & 0 & 0 & C_{44} & C_{45} & 0 \\ 0 & 0 & 0 & C_{45} & C_{55} & 0 \\ C_{16} & C_{26} & C_{36} & 0 & 0 & C_{66} \end{bmatrix}^{(n)} \begin{Bmatrix} \varepsilon_{\theta\theta} \\ \varepsilon_{xx} \\ \varepsilon_{rr} \\ 2\varepsilon_{xr} \\ 2\varepsilon_{r\theta} \\ 2\varepsilon_{\theta x} \end{Bmatrix}^{(n)}$$

$$- \begin{bmatrix} e_{11} & e_{21} & 0 \\ e_{12} & e_{22} & 0 \\ e_{13} & e_{23} & 0 \\ 0 & 0 & e_{34} \\ 0 & 0 & e_{35} \\ e_{16} & e_{26} & 0 \end{bmatrix}^{(n)} \begin{Bmatrix} E_\theta \\ E_x \\ E_r \end{Bmatrix}^{(n)},$$

$$\begin{Bmatrix} D_\theta \\ D_x \\ D_r \end{Bmatrix}^{(n)} = \begin{bmatrix} e_{11} & e_{12} & e_{13} & 0 & 0 & e_{16} \\ e_{21} & e_{22} & e_{23} & 0 & 0 & e_{26} \\ 0 & 0 & 0 & e_{34} & e_{35} & 0 \end{bmatrix}^{(n)} \begin{Bmatrix} \varepsilon_{\theta\theta} \\ \varepsilon_{xx} \\ \varepsilon_{rr} \\ 2\varepsilon_{xr} \\ 2\varepsilon_{r\theta} \\ 2\varepsilon_{\theta x} \end{Bmatrix}^{(n)} + \begin{bmatrix} \epsilon_{11} & \epsilon_{12} & 0 \\ \epsilon_{12} & \epsilon_{22} & 0 \\ 0 & 0 & \epsilon_{33} \end{bmatrix}^{(n)} \begin{Bmatrix} E_\theta \\ E_x \\ E_r \end{Bmatrix}^{(n)}, \quad (2)$$

where ε denotes the infinitesimal strain tensor, E the electric field vector, C_{ij} are the elasticity constants, e_{ij} the piezoelectric moduli,

and ϵ_{ij} the electric permittivity. Material elasticities and permittivities are assumed to yield a positive stored energy density for every non-rigid deformation and/or non-zero electric field [28]. For an elastic layer, the piezoelectric moduli e_{ij} are identically zero. The infinitesimal strain tensor and the electric field are related to the mechanical displacements u and the electric potential ϕ by

$$\begin{aligned}\epsilon_{\theta\theta}^{(n)} &= \frac{1}{r}(u_{\theta,\theta}^{(n)} + u_r^{(n)}), \\ \epsilon_{xx}^{(n)} &= u_{x,x}^{(n)}, \quad \epsilon_{rr}^{(n)} = u_{r,r}^{(n)}, \quad \epsilon_{xr}^{(n)} = \frac{1}{2}(u_{r,x}^{(n)} + u_{x,r}^{(n)}), \\ \epsilon_{r\theta}^{(n)} &= \frac{1}{2}\left(\frac{1}{r}u_{r,\theta}^{(n)} + u_{\theta,r}^{(n)} - \frac{u_\theta^{(n)}}{r}\right), \quad \epsilon_{\theta x}^{(n)} = \frac{1}{2}\left(u_{\theta,x}^{(n)} + \frac{1}{r}u_{x,\theta}^{(n)}\right), \\ E_\theta^{(n)} &= -\frac{1}{r}\phi_{,\theta}^{(n)}, \quad E_r^{(n)} = -\phi_{,r}^{(n)}, \quad E_x^{(n)} = -\phi_{,x}^{(n)}.\end{aligned}\quad (3)$$

The edges $\theta=0$ and Θ are assumed to be mechanically simply supported and free of electric charge, resulting in the following boundary conditions:

$$\sigma_{\theta\theta}^{(n)} = \sigma_{\theta x}^{(n)} = 0, \quad u_r^{(n)} = 0, \quad D_\theta^{(n)} = 0 \quad \text{at } \theta=0, \Theta. \quad (4)$$

Analytical solutions for laminated shells can be obtained only for certain combinations of boundary conditions on the edges. Chen and Shen [12] assumed the edges to be electrically grounded ($\phi^{(n)}=0$) in order to obtain analytical solutions for hybrid laminates with radially poled piezoelectric actuators. In the case of circumferentially poled piezoelectric shear actuators, we assume that the edges are free of electric charge ($D_\theta^{(n)}=0$) in order to obtain an analytical solution.

The boundary conditions prescribed on the inner and outer surfaces of the shell consist of either a mechanical displacement component or the traction component in each of the coordinate directions. In addition, either the electric potential or the normal component of the electric displacement has to be prescribed. Typically non-zero normal tractions and electric potential are prescribed on the inner and outer surfaces of a shell. Since any function can be expanded in terms of a Fourier series, it is sufficient to consider the following electrical and/or mechanical loads on the outer surface $r=R+H/2$ of the hybrid shell

$$\begin{aligned}\sigma_{rr}\left(\theta, R + \frac{H}{2}\right) &= q_0 e^{i\omega t} \sin \frac{k\pi\theta}{\Theta}, \\ \sigma_{r\theta}\left(\theta, R + \frac{H}{2}\right) &= \sigma_{rx}\left(\theta, R + \frac{H}{2}\right) = 0, \\ \phi\left(\theta, R + \frac{H}{2}\right) &= \phi_0 e^{i\omega t} \cos \frac{k\pi\theta}{\Theta},\end{aligned}\quad (5)$$

where k is a non-negative integer and ω denotes the circular frequency. Similar boundary conditions are specified on the inner surface $r=R-H/2$ of the hybrid shell.

The interface conditions on the material surfaces $r=r^{(2)}, \dots, r^{(N)}$ may be specified as follows.

(a) If the surface $r=r^{(n+1)}$ is an interface between two laminae, the mechanical displacements, surface tractions, the electric potential, and the normal component of the electric displacement between them are continuous. That is

$$\begin{aligned}\llbracket u_r, u_\theta, u_x \rrbracket &= 0, \quad \llbracket \sigma_{rr}, \sigma_{r\theta}, \sigma_{rx} \rrbracket = 0, \quad \llbracket \phi \rrbracket = 0, \\ \llbracket D_r \rrbracket &= 0 \quad \text{at } r=r^{(n+1)},\end{aligned}\quad (6)$$

where $\llbracket u_r \rrbracket = u_r^{(n+1)} - u_r^{(n)}$ denotes the jump in the value of u_r across the interface. Thus the adjoining laminae are presumed to be me-

chanically and electrically perfectly bonded together.

(b) If the interface $r=r^{(n+1)}$ is electroded, then the electric potential on this surface is assumed to be a known function of the form $\phi_0^{(n+1)} e^{i\omega t} \cos k\pi\theta/\Theta$. The normal component of the electric displacement need not be continuous across this interface. Thus

$$\begin{aligned}\llbracket u_r, u_\theta, u_x \rrbracket &= 0, \quad \llbracket \sigma_{rr}, \sigma_{r\theta}, \sigma_{rx} \rrbracket = 0, \\ \phi^{(n)} &= \phi^{(n+1)} = \phi_0^{(n+1)} e^{i\omega t} \cos \frac{k\pi\theta}{\Theta} \quad \text{at } r=r^{(n+1)}.\end{aligned}\quad (7)$$

3 An Analytical Solution

We postulate that the displacements and electric potential are functions of r and θ only. Thus the hybrid laminate is in a generalized plane strain state of deformation. This assumption is reasonable because the applied loads and material properties are independent of x , and the body is of infinite extent in the x direction.

We seek a semi-inverse solution by assuming the following forms for the displacements and electric potential:

$$\begin{aligned}u_\theta^{(n)}(\theta, r, t) &= U_\theta^{(n)}(r) e^{i\omega t} \cos p\theta, \\ u_x^{(n)}(\theta, r, t) &= U_x^{(n)}(r) e^{i\omega t} \cos p\theta, \\ u_r^{(n)}(\theta, r, t) &= U_r^{(n)}(r) e^{i\omega t} \sin p\theta, \\ \phi^{(n)}(\theta, r, t) &= \Phi^{(n)}(r) e^{i\omega t} \cos p\theta,\end{aligned}\quad (8)$$

where $p=k\pi/\Theta$. The assumed displacement field satisfies the boundary conditions (4) u_r at the edges $\theta=0, \Theta$.

Substitution of Eq. (8) into Eq. (3) and the result into Eq. (2) yields the following expressions for the stresses and electric displacements:

$$\begin{aligned}\sigma_{\theta\theta}^{(n)} &= \left(C_{11}^{(n)} \frac{U_r^{(n)} - pU_\theta^{(n)}}{r} + C_{13}^{(n)} \frac{dU_r^{(n)}}{dr} - C_{16}^{(n)} \frac{pU_x^{(n)}}{r} \right. \\ &\quad \left. - e_{11}^{(n)} \frac{\Phi^{(n)} p}{r} \right) e^{i\omega t} \sin p\theta, \\ \sigma_{xx}^{(n)} &= \left(C_{12}^{(n)} \frac{U_r^{(n)} - pU_\theta^{(n)}}{r} + C_{23}^{(n)} \frac{dU_r^{(n)}}{dr} - C_{26}^{(n)} \frac{pU_x^{(n)}}{r} \right. \\ &\quad \left. - e_{12}^{(n)} \frac{\Phi^{(n)} p}{r} \right) e^{i\omega t} \sin p\theta, \\ \sigma_{rr}^{(n)} &= \left(C_{13}^{(n)} \frac{U_r^{(n)} - pU_\theta^{(n)}}{r} + C_{33}^{(n)} \frac{dU_r^{(n)}}{dr} - C_{36}^{(n)} \frac{pU_x^{(n)}}{r} \right. \\ &\quad \left. - e_{13}^{(n)} \frac{\Phi^{(n)} p}{r} \right) e^{i\omega t} \sin p\theta, \\ \sigma_{xr}^{(n)} &= \left(C_{44}^{(n)} \frac{dU_x^{(n)}}{dr} + C_{45}^{(n)} \frac{U_r^{(n)} p - U_\theta^{(n)}}{r} + C_{45}^{(n)} \frac{dU_\theta^{(n)}}{dr} \right. \\ &\quad \left. + e_{34}^{(n)} \frac{d\Phi^{(n)}}{dr} \right) e^{i\omega t} \cos p\theta, \\ \sigma_{r\theta}^{(n)} &= \left(C_{45}^{(n)} \frac{dU_x^{(n)}}{dr} + C_{55}^{(n)} \frac{U_r^{(n)} p - U_\theta^{(n)}}{r} + C_{55}^{(n)} \frac{dU_\theta^{(n)}}{dr} \right. \\ &\quad \left. + e_{35}^{(n)} \frac{d\Phi^{(n)}}{dr} \right) e^{i\omega t} \cos p\theta,\end{aligned}$$

$$\begin{aligned}
\sigma_{\theta x}^{(n)} &= \left(C_{16}^{(n)} \frac{U_r^{(n)} - pU_\theta^{(n)}}{r} + C_{36}^{(n)} \frac{dU_r^{(n)}}{dr} - C_{66}^{(n)} \frac{pU_x^{(n)}}{r} \right. \\
&\quad \left. - e_{16}^{(n)} \frac{\Phi^{(n)} p}{r} \right) e^{i\omega t} \sin p\theta, \\
D_\theta^{(n)} &= \left(e_{11}^{(n)} \frac{U_r^{(n)} - pU_\theta^{(n)}}{r} + e_{13}^{(n)} \frac{dU_r^{(n)}}{dr} - e_{16}^{(n)} \frac{pU_x^{(n)}}{r} \right. \\
&\quad \left. + \epsilon_{11}^{(n)} \frac{\Phi^{(n)} p}{r} \right) e^{i\omega t} \sin p\theta, \\
D_x^{(n)} &= \left(e_{21}^{(n)} \frac{U_r^{(n)} - pU_\theta^{(n)}}{r} + e_{23}^{(n)} \frac{dU_r^{(n)}}{dr} - e_{26}^{(n)} \frac{pU_x^{(n)}}{r} \right. \\
&\quad \left. + \epsilon_{21}^{(n)} \frac{\Phi^{(n)} p}{r} \right) e^{i\omega t} \sin p\theta, \\
D_r^{(n)} &= \left(e_{34}^{(n)} \frac{dU_x^{(n)}}{dr} + e_{35}^{(n)} \frac{U_r^{(n)} p - U_\theta^{(n)}}{r} + e_{35}^{(n)} \frac{dU_\theta^{(n)}}{dr} \right. \\
&\quad \left. - \epsilon_{33}^{(n)} \frac{d\Phi^{(n)}}{dr} \right) e^{i\omega t} \cos p\theta. \tag{9}
\end{aligned}$$

An examination of Eq. (9) reveals that the stress components $\sigma_{\theta\theta}$ and $\sigma_{\theta x}$ and the electric displacement D_θ satisfy the boundary conditions (4) at the edges $\theta=0$ and Θ .

Substitution of Eq. (9) into the governing equations (1) yields four coupled second-order ordinary differential equations for $U_r^{(n)}(r)$, $U_\theta^{(n)}(r)$, $U_x^{(n)}(r)$ and $\Phi^{(n)}(r)$,

$$\begin{aligned}
C_{13}^{(n)} r \frac{dU_r^{(n)}}{dr} - (C_{13}^{(n)} + C_{55}^{(n)}) p r \frac{dU_\theta^{(n)}}{dr} + C_{33}^{(n)} r^2 \frac{d^2 U_r^{(n)}}{dr^2} - (C_{36}^{(n)} \\
+ C_{45}^{(n)}) p r \frac{dU_x^{(n)}}{dr} - (e_{13}^{(n)} + e_{35}^{(n)}) p r \frac{d\Phi^{(n)}}{dr} - C_{55}^{(n)} p (pU_r^{(n)} - U_\theta^{(n)}) \\
+ (C_{33}^{(n)} - C_{13}^{(n)}) r \frac{dU_r^{(n)}}{dr} - C_{11}^{(n)} (U_r^{(n)} - pU_\theta^{(n)}) + C_{16}^{(n)} p U_x^{(n)} \\
+ e_{11}^{(n)} p \Phi^{(n)} + \rho^{(n)} \omega^2 r^2 U_r^{(n)} = 0, \\
C_{45}^{(n)} r^2 \frac{d^2 U_x^{(n)}}{dr^2} + (C_{13}^{(n)} + C_{55}^{(n)}) p r \frac{dU_r^{(n)}}{dr} + C_{55}^{(n)} r^2 \frac{d^2 U_\theta^{(n)}}{dr^2} + e_{35}^{(n)} r^2 \frac{d^2 \Phi^{(n)}}{dr^2} \\
+ C_{11}^{(n)} p (U_r^{(n)} - pU_\theta^{(n)}) - C_{16}^{(n)} p^2 U_x^{(n)} - e_{11}^{(n)} p^2 \Phi^{(n)} + 2C_{45}^{(n)} r \frac{dU_x^{(n)}}{dr} \\
+ C_{55}^{(n)} (pU_r^{(n)} - U_\theta^{(n)}) + C_{55}^{(n)} r \frac{dU_\theta^{(n)}}{dr} + 2e_{35}^{(n)} r \frac{d\Phi^{(n)}}{dr} + \rho^{(n)} \omega^2 r^2 U_\theta^{(n)}
\end{aligned}$$

$$\mathbf{M}^{(n)}(\beta) = \begin{bmatrix} -C_{11}^{(n)} - C_{55}^{(n)} p^2 + C_{33}^{(n)} (\beta + \lambda^{(n)})^2 & C_{11}^{(n)} p + C_{55}^{(n)} p - (C_{13}^{(n)} + C_{55}^{(n)}) p (\beta + \lambda^{(n)}) & C_{16}^{(n)} p - (C_{36}^{(n)} + C_{45}^{(n)}) p (\beta + \lambda^{(n)}) & e_{11}^{(n)} p - (e_{13}^{(n)} + e_{35}^{(n)}) p (\beta + \lambda^{(n)}) \\ C_{11}^{(n)} p + C_{13}^{(n)} p (\beta + \lambda^{(n)}) + C_{55}^{(n)} p (\beta + \lambda^{(n)} + 1) & -C_{11}^{(n)} p^2 + C_{55}^{(n)} p (\beta + \lambda^{(n)} + 1) (\beta + \lambda^{(n)} - 1) & -e_{16}^{(n)} p^2 + C_{45}^{(n)} (\beta + \lambda^{(n)} + 1) (\beta + \lambda^{(n)}) & -e_{11}^{(n)} p^2 + e_{35}^{(n)} (\beta + \lambda^{(n)} + 1) (\beta + \lambda^{(n)}) \\ C_{16}^{(n)} p + (C_{36}^{(n)} + C_{45}^{(n)}) p (\beta + \lambda^{(n)}) & -C_{16}^{(n)} p^2 + C_{45}^{(n)} (\beta + \lambda^{(n)}) (\beta + \lambda^{(n)} - 1) & -C_{66}^{(n)} p^2 + C_{44}^{(n)} (\beta + \lambda^{(n)})^2 & -e_{16}^{(n)} p^2 + e_{35}^{(n)} (\beta + \lambda^{(n)}) + e_{34}^{(n)} (\beta + \lambda^{(n)}) (\beta + \lambda^{(n)} - 1) \\ e_{11}^{(n)} p + (e_{13}^{(n)} + e_{35}^{(n)}) p (\beta + \lambda^{(n)}) & -e_{11}^{(n)} p^2 + e_{35}^{(n)} (\beta + \lambda^{(n)}) (\beta + \lambda^{(n)} - 1) & -e_{16}^{(n)} p^2 + e_{34}^{(n)} (\beta + \lambda^{(n)})^2 & \epsilon_{11}^{(n)} p^2 - \epsilon_{33}^{(n)} (\beta + \lambda^{(n)})^2 \end{bmatrix} \tag{13}$$

A non-trivial solution for $\{A_r^{(n,0)}, A_\theta^{(n,0)}, A_x^{(n,0)}, A_\phi^{(n,0)}\}$ is obtained by setting the determinant of the matrix in Eq. (12) to zero

$$|\mathbf{M}^{(n)}(0)| = 0. \tag{14}$$

Equation (14) is the *indicial equation* for the differential equations (10). Since the determinant of $\mathbf{M}^{(n)}(0)$ is an eighth-order polynomial in the exponent $\lambda^{(n)}$, we obtain eight roots $\lambda_m^{(n)}$, $m=1, \dots, 8$.

$$\begin{aligned}
&= 0, \\
C_{44}^{(n)} r^2 \frac{d^2 U_x^{(n)}}{dr^2} + (C_{45}^{(n)} + C_{36}^{(n)}) p r \frac{dU_r^{(n)}}{dr} + C_{45}^{(n)} r^2 \frac{d^2 U_\theta^{(n)}}{dr^2} + e_{34}^{(n)} r^2 \frac{d^2 \Phi^{(n)}}{dr^2} \\
&\quad + C_{16}^{(n)} p (U_r^{(n)} - pU_\theta^{(n)}) - C_{66}^{(n)} p^2 U_x^{(n)} - e_{16}^{(n)} p^2 \Phi^{(n)} + C_{44}^{(n)} r \frac{dU_x^{(n)}}{dr} \\
&\quad + e_{35}^{(n)} r \frac{d\Phi^{(n)}}{dr} + \rho^{(n)} \omega^2 r^2 U_x^{(n)} = 0, \\
e_{34}^{(n)} r^2 \frac{d^2 U_x^{(n)}}{dr^2} + (e_{13}^{(n)} + e_{35}^{(n)}) p r \frac{dU_r^{(n)}}{dr} + e_{35}^{(n)} r^2 \frac{d^2 U_\theta^{(n)}}{dr^2} - \epsilon_{33}^{(n)} r^2 \frac{d^2 \Phi^{(n)}}{dr^2} \\
&\quad + e_{11}^{(n)} p (U_r^{(n)} - pU_\theta^{(n)}) - e_{16}^{(n)} p^2 U_x^{(n)} + \epsilon_{11}^{(n)} p^2 \Phi^{(n)} + e_{34}^{(n)} r \frac{dU_x^{(n)}}{dr} \\
&\quad - \epsilon_{33}^{(n)} r \frac{d\Phi^{(n)}}{dr} = 0.
\end{aligned}$$

A solution to the differential equations (10) is sought by the Frobenius method [29]. The functions $U_r^{(n)}(r)$, $U_\theta^{(n)}(r)$, $U_x^{(n)}(r)$, and $\Phi^{(n)}(r)$ are assumed to have the following series solution:

$$\begin{aligned}
U_\theta^{(n)}(r) &= r^{\lambda^{(n)}} \sum_{\beta=0}^{\infty} A_\theta^{(n,\beta)} r^\beta, & U_x^{(n)}(r) &= r^{\lambda^{(n)}} \sum_{\beta=0}^{\infty} A_x^{(n,\beta)} r^\beta, \\
U_r^{(n)}(r) &= r^{\lambda^{(n)}} \sum_{\beta=0}^{\infty} A_r^{(n,\beta)} r^\beta, & \Phi^{(n)}(r) &= r^{\lambda^{(n)}} \sum_{\beta=0}^{\infty} A_\phi^{(n,\beta)} r^\beta, \tag{11}
\end{aligned}$$

where the exponent $\lambda^{(n)}$ may be any real or complex number and it is chosen such that either $A_r^{(n,0)}$, $A_\theta^{(n,0)}$, $A_x^{(n,0)}$, or $A_\phi^{(n,0)}$ is non-zero. Note that the latter condition is no restriction of generality since it simply means that we factor out the highest possible power of r . Inserting (11) into the differential equations (10) and equating like powers of $r^{\lambda^{(n)}}$ on both sides of the equations results in

$$\mathbf{M}^{(n)}(0) \begin{Bmatrix} A_r^{(n,0)} \\ A_\theta^{(n,0)} \\ A_x^{(n,0)} \\ A_\phi^{(n,0)} \end{Bmatrix} = \begin{Bmatrix} 0 \\ 0 \\ 0 \\ 0 \end{Bmatrix}, \tag{12}$$

where the matrix $\mathbf{M}^{(n)}(\beta)$ is

The eigenvector of coefficients $\{A_r^{(n,0)}, A_\theta^{(n,0)}, A_x^{(n,0)}, A_\phi^{(n,0)}\}$ associated with each of the eight exponents $\lambda_m^{(n)}$ is determined from the nullspace of $\mathbf{M}^{(n)}(0)$ after setting $\lambda^{(n)} = \lambda_m^{(n)}$. It is assumed that the exponents $\lambda_m^{(n)}$ are distinct and do not differ by an integer value. In the mathematically degenerate cases of repeated exponents or exponents that differ by an integer, the solution (11) needs to be modified appropriately [29].

Table 1 Non-vanishing material properties of graphite-epoxy and PZT-5A shear actuators

Property	0° graphite-epoxy	±45° graphite-epoxy	PZT-5A
C_{11} (GPa)	183.443	58.128	86.856
C_{22} (GPa)	11.662	58.128	99.201
C_{33} (GPa)	11.662	11.662	99.201
C_{12} (GPa)	4.363	43.788	50.778
C_{13} (GPa)	4.363	4.140	50.778
C_{23} (GPa)	3.918	4.140	54.016
C_{44} (GPa)	2.870	5.020	22.600
C_{55} (GPa)	7.170	5.020	21.100
C_{66} (GPa)	7.170	46.595	21.100
C_{16} (GPa)	0	±42.945	0
C_{26} (GPa)	0	±42.945	0
C_{36} (GPa)	0	±0.222	0
C_{45} (GPa)	0	±2.150	0
e_{11} (Cm ⁻²)	0	0	15.118
e_{12} (Cm ⁻²)	0	0	-7.209
e_{13} (Cm ⁻²)	0	0	-7.209
e_{26} (Cm ⁻²)	0	0	12.322
e_{35} (Cm ⁻²)	0	0	12.322
ϵ_{11} (10 ⁻¹⁰ F/m)	153.0	153.0	150.0
ϵ_{22} (10 ⁻¹⁰ F/m)	153.0	153.0	153.0
ϵ_{33} (10 ⁻¹⁰ F/m)	153.0	153.0	153.0
ρ (kg/m ³)	1590	1590	7750

Inserting Eq. (11) into the differential equations (10) and equating like powers of $r^{\lambda^{(n)}+1}$ on both sides of the equations results in equation for the series coefficients $A_r^{(n,1)}$, $A_\theta^{(n,1)}$, $A_x^{(n,1)}$, and $A_\phi^{(n,1)}$,

$$\begin{Bmatrix} A_r^{(n,1)} \\ A_\theta^{(n,1)} \\ A_x^{(n,1)} \\ A_\phi^{(n,1)} \end{Bmatrix} = (\mathbf{M}^{(n)}(1))^{-1} \begin{Bmatrix} 0 \\ 0 \\ 0 \\ 0 \end{Bmatrix} = \begin{Bmatrix} 0 \\ 0 \\ 0 \\ 0 \end{Bmatrix}. \quad (15)$$

It should be noted that $\mathbf{M}^{(n)}(1)$ in Eq. (15) is invertible when the exponents $\lambda_m^{(n)}$ are distinct and do not differ by an integer value. Similarly, equating like powers of $r^{\lambda^{(n)}+\beta}$ ($\beta \geq 2$) results in the following recurrence relations for the series coefficients $A_r^{(n,\beta)}$, $A_\theta^{(n,\beta)}$, $A_x^{(n,\beta)}$, and $A_\phi^{(n,\beta)}$:

$$\begin{Bmatrix} A_r^{(n,\beta)} \\ A_\theta^{(n,\beta)} \\ A_x^{(n,\beta)} \\ A_\phi^{(n,\beta)} \end{Bmatrix} = (\mathbf{M}^{(n)}(\beta))^{-1} \begin{Bmatrix} -\rho^{(n)} \omega^2 A_r^{(n,\beta-2)} \\ -\rho^{(n)} \omega^2 A_\theta^{(n,\beta-2)} \\ -\rho^{(n)} \omega^2 A_x^{(n,\beta-2)} \\ 0 \end{Bmatrix}. \quad (16)$$

The recurrence relation (16) is evaluated successively for $\beta = 2, 3, \dots$, to obtain the series coefficients $A_r^{(n,\beta)}$, $A_\theta^{(n,\beta)}$, $A_x^{(n,\beta)}$, and $A_\phi^{(n,\beta)}$. The complete solution, obtained by a superposition of the solutions corresponding to the eight exponents $\lambda_m^{(n)}$, is

$$\begin{aligned} U_\theta^{(n)}(r) &= \sum_{m=1}^8 \left(B_m^{(n)} \sum_{\beta=0}^{\infty} A_\theta^{(n,\beta)} r^{\beta+\lambda_m^{(n)}} \right), \\ U_x^{(n)}(r) &= \sum_{m=1}^8 \left(B_m^{(n)} \sum_{\beta=0}^{\infty} A_x^{(n,\beta)} r^{\beta+\lambda_m^{(n)}} \right), \\ U_r^{(n)}(r) &= \sum_{m=1}^8 \left(B_m^{(n)} \sum_{\beta=0}^{\infty} A_r^{(n,\beta)} r^{\beta+\lambda_m^{(n)}} \right), \\ \Phi^{(n)}(r) &= \sum_{m=1}^8 \left(B_m^{(n)} \sum_{\beta=0}^{\infty} A_\phi^{(n,\beta)} r^{\beta+\lambda_m^{(n)}} \right), \end{aligned} \quad (17)$$

where $B_m^{(n)}$ are constants.

3.1 Static Deformation and Forced Vibration Analysis. If the hybrid laminate is subjected to a static or time harmonic load, the angular frequency ω and k are known. The constants $B_m^{(n)}$ are obtained by applying four boundary conditions on the outer surface (5), four conditions on the inner surface of the laminate, and eight interface conditions (6) or (7) at each of the $(N-1)$ interfaces between the N laminae, which leads to the following matrix equation:

$$\mathbf{G}(\omega)\mathbf{B} = \mathbf{W}, \quad (18)$$

where $\mathbf{G}(\omega)$ is a known $8N \times 8N$ matrix, \mathbf{W} is a known vector of length $8N$, and \mathbf{B} is a vector consisting of the $8N$ constants $B_m^{(n)}$. The linear system of equations (18) is solved to obtain the $8N$ constants $B_m^{(n)}$ and hence the solution for every layer. In the case of static deformation the angular frequency $\omega=0$.

3.2 Free Vibration Analysis. The hybrid composite shell is in a state of free vibration if it is not subjected to any applied

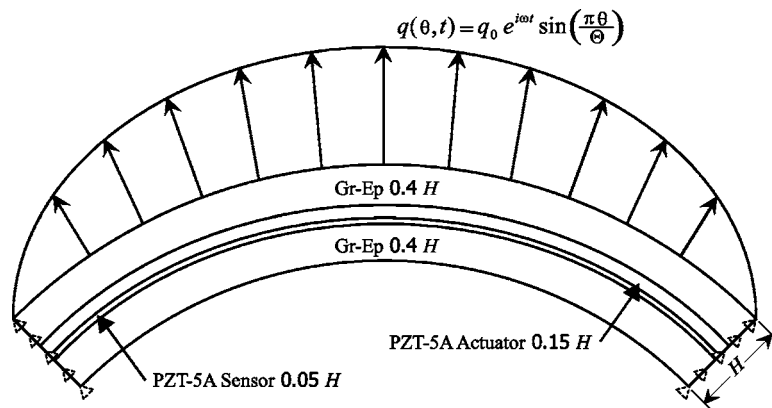


Fig. 2 A four-layer hybrid shell with piezoelectric sensor and actuator sandwiched between fiber-reinforced composite layers

Table 2 Convergence study for a [0° Gr-Ep/PZT-5A/PZT-5A/0° Gr-Ep] hybrid cylindrical shell for $R=0.25$ m and $R/H=5$

K	Mode $\omega_1^{(1)}$				Mode $\omega_1^{(3)}$			
	$\omega_1^{(1)}$	$\phi(0,R)e_0$		$\sigma_{r\theta}(0,R+H/4)R$	$\omega_1^{(3)}$	$\phi(0,R)e_0$		$\sigma_{r\theta}(0,R+H/4)R$
		$C_0 u_r(\Theta/(2k), R+H/2)$	$u_\theta(0, R+H/2)$			$C_0 u_r(\Theta/(2k), R+H/2)$	$u_r(\Theta/(2k), R+H/2)$	
10	683.229	0.00123365	49.0339	16.6069	2940.68	-7.10804	91.5312	0.835532
20	683.229	0.00123365	49.0339	16.6069	5950.7	12.7256	-289.415	449.412
30	683.229	0.00123365	49.0339	16.6069	8808.68	-5.65086	281.533	-169.985
40	683.229	0.00123365	49.0339	16.6069	10223.9	-1.12821	-399.09	317.062
50	683.229	0.00123365	49.0339	16.6069	10223.9	-1.12821	-399.09	317.063
60	683.229	0.00123365	49.0339	16.6069	10223.9	-1.12821	-399.09	317.063

mechanical or electric loads. For fixed k (i.e., fixed p), the series coefficients $A_r^{(n,\beta)}$, $A_\theta^{(n,\beta)}$, $A_x^{(n,\beta)}$, and $A_\phi^{(n,\beta)}$ are obtained in terms of ω using the recurrence relations (16). Applying the boundary conditions on the outer surface, interfaces between laminae and the inner surfaces of the laminate results in the following homogeneous matrix equation:

$$\mathbf{G}(\omega)\mathbf{B} = \mathbf{0}, \tag{19}$$

where $\mathbf{G}(\omega)$ is an $8N \times 8N$ matrix whose elements are polynomials of ω and \mathbf{B} is a vector consisting of the $8N$ constants $B_m^{(n)}$. A non-trivial solution for the constants $B_m^{(n)}$ is obtained by setting the determinant $|\mathbf{G}(\omega)|$ equal to zero. The resulting polynomial equation is solved to obtain a set of eigenvalues that are arranged in ascending order as $\{\omega_k^{(1)}, \omega_k^{(2)}, \omega_k^{(3)}, \dots\}$, which are the natural frequencies of the shell corresponding to the circumferential mode shape defined by integer k . The eigenvector \mathbf{B} associated with the eigenvalue $\omega_k^{(j)}$ is determined from the nullspace of $\mathbf{G}(\omega_k^{(j)})$. The displacements, electric potential, stresses, and electric displacement at any point within the laminate are determined using the $8N$ constants $B_m^{(n)}$ from the eigenvector \mathbf{B} .

4 Active Damping using Feedback Control

Active damping is implemented through feedback control. The outer surface of the composite shell is subjected to harmonic distributed load

$$\sigma_{rr}^{(N)}(\theta, R+H/2, t) = q_0 e^{i\omega t} \sin \pi\theta/\Theta, \tag{20}$$

where the circular frequency ω is prescribed. We use the positive position feedback (PPF) controller, introduced by Goh and Caughey [25], to achieve active damping. The PPF controller introduces a second-order compensator which is forced by the electric potential of the sensor,

$$\ddot{\eta} + 2\varsigma_c \omega_c \dot{\eta} + \omega_c^2 \eta = \omega_c^2 \phi(0, r_s, t), \tag{21}$$

where r_s is the radial location where the sensor potential is measured, η is the controller coordinate, ω_c is the natural frequency of the controller, and ς_c is the damping ratio of the controller. For steady-state vibration, the controller coordinate is also harmonic $\eta = \eta_0 e^{i\omega t}$ and Eq. (21) becomes

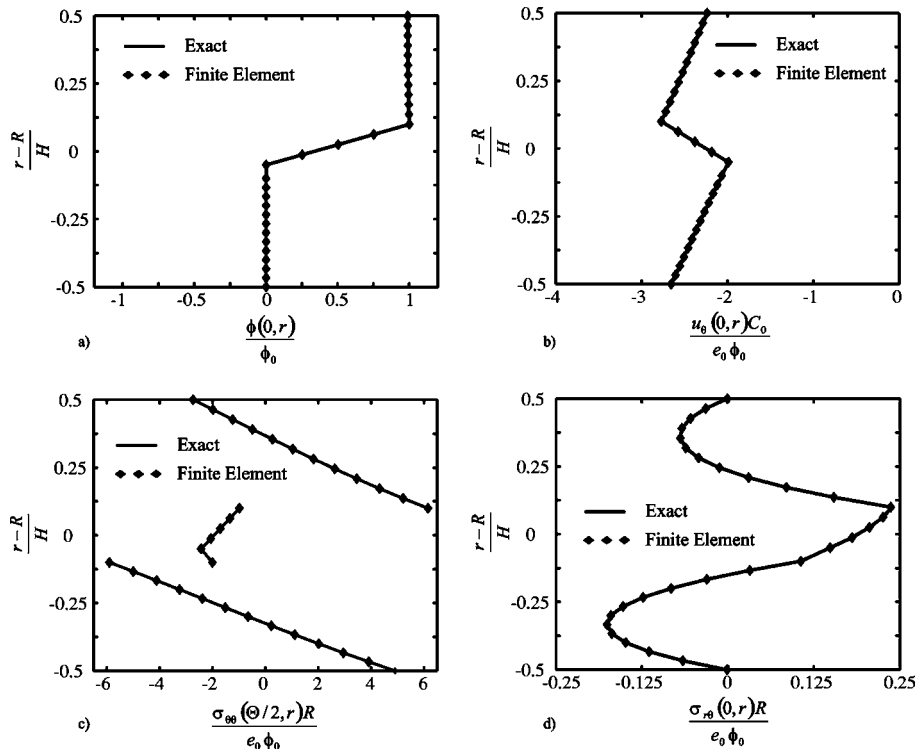


Fig. 3 Comparison of analytical static electric potential, circumferential displacement, circumferential stress, and transverse shear stress with finite element results for an electric potential $\phi(\theta, t) = \phi_0 \cos \pi\theta/\Theta$ applied to the piezoelectric actuator of a four layer hybrid shell

$$-\omega^2 \eta_0 + 2i s_c \omega_c \omega \eta_0 + \omega_c^2 \eta_0 = \omega_c^2 \Phi^{(n_s)}(r_s), \quad (22)$$

where the sensor is lamina n_s . The amplitude of the controller coordinate obtained from Eq. (22) is

$$\eta_0 = \left[\frac{\omega_c^2}{(\omega_c^2 - \omega^2) + 2i s_c \omega_c \omega} \right] \Phi^{(n_s)}(r_s). \quad (23)$$

The controller coordinate η , magnified by a positive gain, is then fed back as a voltage input ϕ to a piezoelectric shear actuator

$$\phi(\theta, t) = g \omega_c^2 \eta \cos \pi \theta / \Theta = \left[\frac{g \omega_c^4 \Phi^{(n_s)}(r_s)}{(\omega_c^2 - \omega^2) + 2i s_c \omega_c \omega} \right] e^{i \omega t} \cos \pi \theta / \Theta, \quad (24)$$

where g is the PPF feedback gain parameter which has units of s^2 .

The feedback potential of the PPF controller (24) is applied as boundary conditions to the piezoelectric shear actuator. The implementation of the other boundary conditions on the top and bottom surfaces of the laminate and the interface conditions is similar to that of forced vibration analysis discussed earlier. Since $\phi(\theta, t)$ and $\Phi^{(n_s)}(r_s)$ are functions of the constants $B_m^{(n)}$, the controller parameter ω_c , s_c and g appear in the left-hand side matrix \mathbf{G} in Eq. (18). The displacements and stresses are complex valued since the feedback potential (24) is complex. The magnitude and phase of the displacements, electric potential, stresses, and electric displacement with respect to the applied harmonic load can be inferred from their respective real and imaginary parts.

In the present analysis, it has been assumed that the fiber-reinforced laminae and piezoelectric layer have no material damping for simplicity. Therefore, any damping of the hybrid laminated shell is a result of the PPF controller. Material damping of the fiber-reinforced laminae can be incorporated using complex elas-

Table 3 First nine natural frequencies of a $[0^\circ \text{ Gr-Ep/PZT-5A/PZT-5A}/0^\circ \text{ Gr-Ep}]$ hybrid cylindrical shell for $R=0.25$ m and $R/H=5$

Mode	Natural Frequency, Hz
$\omega_1^{(1)}$	683.229 (683.23)
$\omega_1^{(2)}$	2393.43 (-)
$\omega_2^{(1)}$	2858.45 (2858.5)
$\omega_2^{(2)}$	4780.83 (-)
$\omega_3^{(1)}$	5254.74 (5254.7)
$\omega_3^{(2)}$	7156.76 (-)
$\omega_4^{(1)}$	7636.58 (7636.6)
$\omega_5^{(1)}$	9984.92 (9984.9)
$\omega_1^{(3)}$	10223.9 (10224)

tic constants C_{ij} . Piezoceramic damping has been incorporated in the analysis of longitudinal vibrations of piezoceramics rods by von Wagner [30,31].

5 Results and Discussion

We present results for hybrid laminates with each lamina made of either fiber-reinforced graphite-epoxy (Gr-Ep) or PZT-5A. The graphite-epoxy is assumed to be orthotropic with its principal material direction inclined at an angle ψ to the θ axis in the θ - x plane. The PZT-5A is assumed to be transversely isotropic with θ axis as the axis of transverse isotropy, which is also the poling direction. The material properties of the circumferentially-poled PZT-5A were obtained by a tensor transformation of the material properties given by Tang et al. [32] of PZT-5A poled in the radial direction. The non-zero values of the material properties are listed in Table 1 for the PZT-5A and graphite-epoxy with fiber orienta-

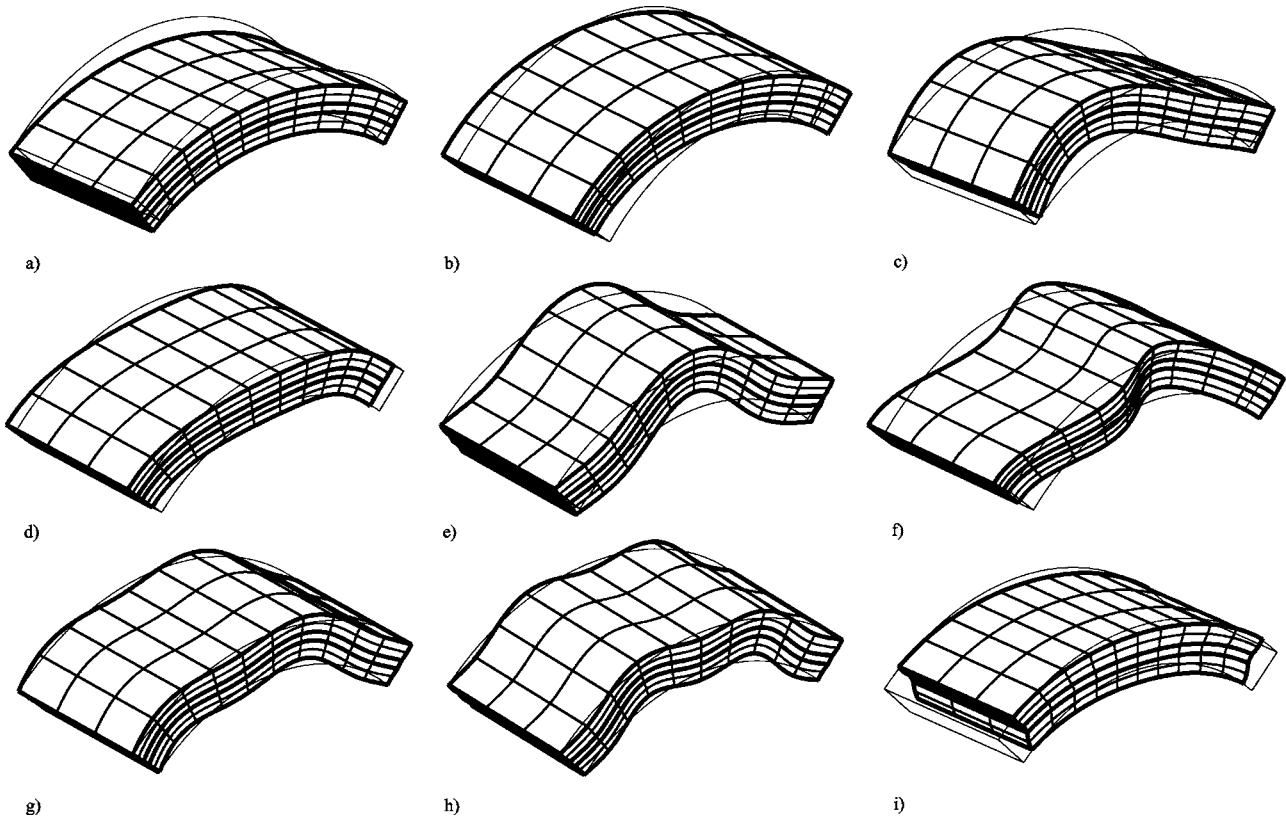


Fig. 4 First nine mode shapes for a $[0^\circ \text{ Gr-Ep/PZT-5A/PZT-5A}/0^\circ \text{ Gr-Ep}]$ hybrid shell, electrically closed, $R=0.25$ m, $R/H=5$: (a) $\omega_1^{(1)}=683.229$ Hz, (b) $\omega_1^{(2)}=2393.43$ Hz, (c) $\omega_2^{(1)}=2858.45$ Hz, (d) $\omega_2^{(2)}=4780.83$ Hz, (e) $\omega_3^{(1)}=5254.74$ Hz, (f) $\omega_3^{(2)}=7156.76$ Hz, (g) $\omega_4^{(1)}=7636.58$ Hz, (h) $\omega_5^{(1)}=9984.92$ Hz, and (i) $\omega_1^{(3)}=10223.9$ Hz

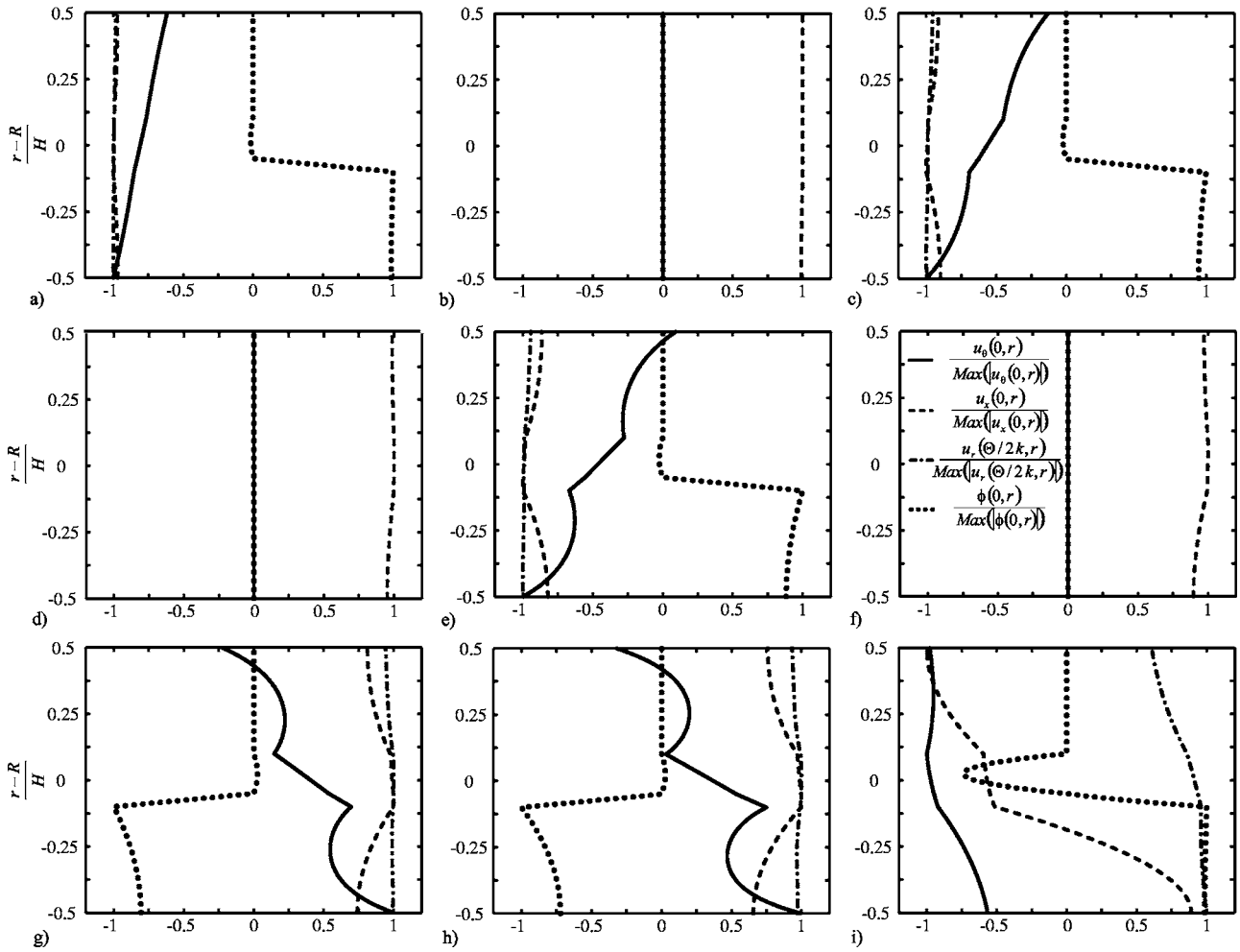


Fig. 5 The displacement and electric potential as a function of the radial coordinate for the first nine modes of a $[0^\circ \text{ Gr-Ep/PZT-5A/PZT-5A}/0^\circ \text{ Gr-Ep}]$ hybrid shell, $R=0.25 \text{ m}$, $R/H=5$: (a) $\omega_1^{(1)}=683.229 \text{ Hz}$, (b) $\omega_1^{(2)}=2393.43 \text{ Hz}$, (c) $\omega_2^{(1)}=2858.45 \text{ Hz}$, (d) $\omega_2^{(2)}=4780.83 \text{ Hz}$, (e) $\omega_3^{(1)}=5254.74 \text{ Hz}$, (f) $\omega_3^{(2)}=7156.76 \text{ Hz}$, (g) $\omega_4^{(1)}=7636.58 \text{ Hz}$, (h) $\omega_5^{(1)}=9984.92 \text{ Hz}$, and (i) $\omega_5^{(3)}=10223.9 \text{ Hz}$

tions $\psi=0^\circ$ and $\pm 45^\circ$. In our analysis, we consider all the layers, including graphite-epoxy, to be piezoelectric with the piezoelectric moduli of graphite-epoxy set equal to zero.

All results presented in this work are for four layer hybrid cylindrical shells depicted in Fig. 2. The radial location of the mid-surface of the hybrid shell is $R=0.25 \text{ m}$ and the thickness of the shell $H=R/5$. The inner and outer layers ($n=1,4$) are made of fiber-reinforced materials of thickness $0.4H$ that sandwich a piezoelectric sensor ($n=2$) of thickness $0.05H$ and a piezoelectric actuator ($n=3$) of thickness $0.15H$. The radial locations of the inner surface, interfaces and outer surface are $r^{(1)}=R-0.5H$, $r^{(2)}=R-0.1H$, $r^{(3)}=R-0.05H$, $r^{(4)}=R+0.1H$, and $r^{(5)}=R+0.5H$. The bottom surface of the sensor at $r=r^{(2)}$ is perfectly bonded and conditions (6) are applied. The outer surface of the piezoelectric actuator is electroded and interface conditions (7) are applied at $r=r^{(4)}$. The interface between the sensor and actuator at $r=r^{(3)}$ is electrically grounded and conditions (7) are enforced with $\phi_0=0$.

The effect of truncation of the series on the accuracy of the natural frequencies, displacements, electric potential and stresses is investigated by computing the solution at specific points in a $[0^\circ \text{ Gr-Ep/PZT-5A/PZT-5A}/0^\circ \text{ Gr-Ep}]$ hybrid shell. The natural frequencies $\omega_1^{(1)}$ and $\omega_1^{(3)}$ and the corresponding electric potential, displacements, and stresses at specific points of the piezoelectric composite shell are listed in Table 2 for increasing number of terms K . These results show that the natural frequencies, mechani-

cal displacements, stresses, and electric potential converge rapidly. Based on this convergence study, we use 60 terms in the series solution (11) to obtain accurate results.

5.1 Static Deformation. We consider the static deformation of a hybrid laminate with inner and outer laminae made of 0° graphite-epoxy, i.e., a $[0^\circ \text{ Gr-Ep/PZT-5A/PZT-5A}/0^\circ \text{ Gr-Ep}]$ laminate. An electric potential $\phi=\phi_0 \cos \pi\theta/\Theta$ is applied to the electroded interface $r=r^{(4)}$ between the piezoelectric actuator and the outer graphite-epoxy layer. There is good comparison of the static displacement, electric potential, and stresses of the analytical solution with a plane strain finite element solution, as shown in Fig. 3. This ensures that there are no algebraic errors in the implementation of the analytical solution. The plane strain finite element solution is obtained using the commercial finite element program ABAQUS/Standard 6.3-1 [33] with 5600 eight-node biquadratic elements and 17257 nodes. The electric load to the piezoelectric actuator causes the shell to deflect radially inward and causes a zig-zag displacement u_θ in the circumferential direction as shown in Fig. 3(b). Due to the elastic coupling between the radial displacement and the circumferential displacement, the shell exhibits a non-zero average circumferential displacement u_θ , unlike a hybrid flat plate [21]. The maximum value of the transverse shear stress occurs at the interface between the piezoelectric shear actuator and the outer graphite-epoxy layer [Fig. 3(d)].

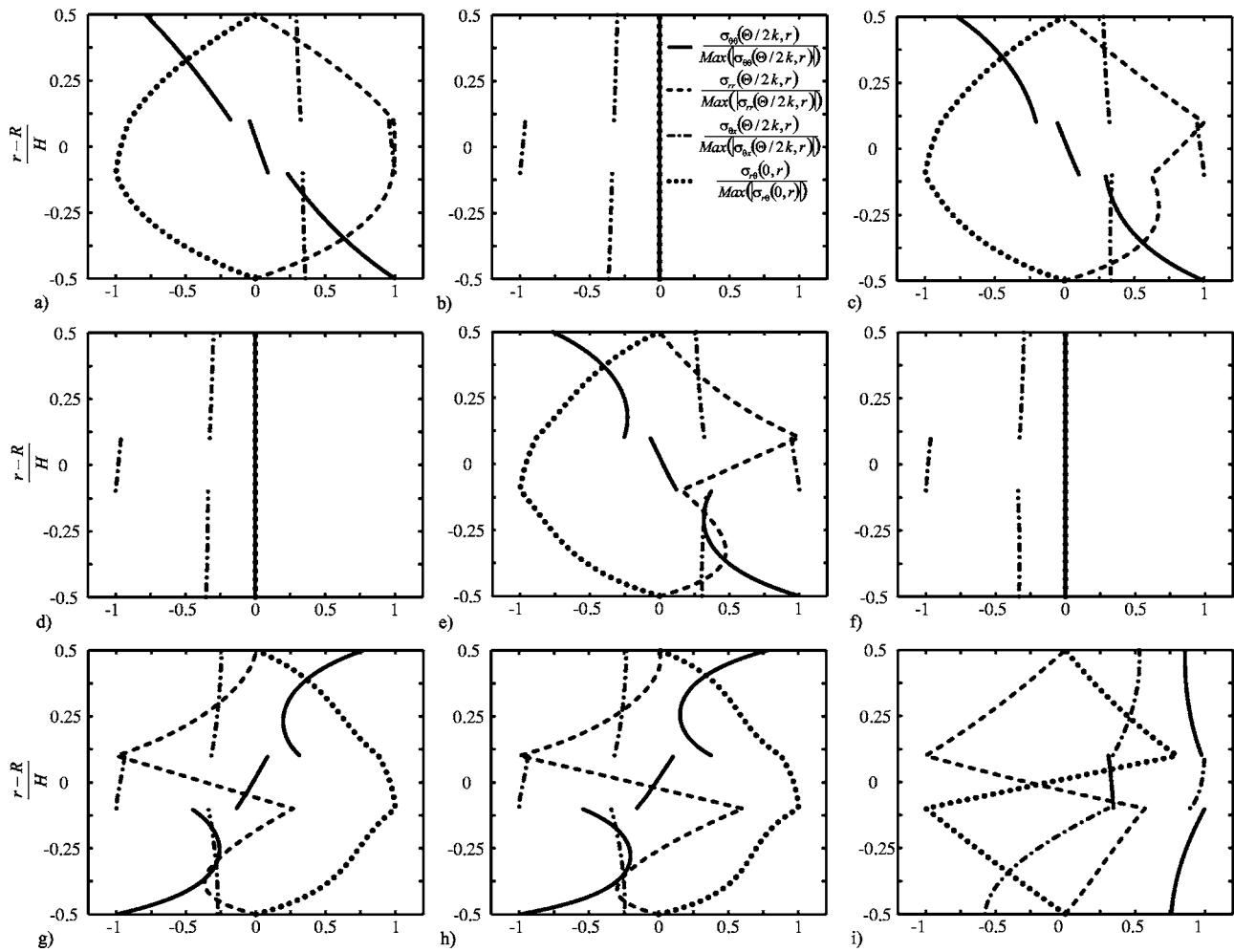


Fig. 6 The stresses as a function of the radial coordinate for the first nine modes of a $[0^\circ \text{ Gr-Ep/PZT-5A/PZT-5A}/0^\circ \text{ Gr-Ep}]$ hybrid shell, $R=0.25 \text{ m}$, $R/H=5$: (a) $\omega_1^{(1)}=683.229 \text{ Hz}$, (b) $\omega_1^{(2)}=2393.43 \text{ Hz}$, (c) $\omega_1^{(1)}=2858.45 \text{ Hz}$, (d) $\omega_2^{(2)}=4780.83 \text{ Hz}$, (e) $\omega_3^{(1)}=5254.74 \text{ Hz}$, (f) $\omega_2^{(2)}=7156.76 \text{ Hz}$, (g) $\omega_4^{(1)}=7636.58 \text{ Hz}$, (h) $\omega_1^{(1)}=9984.92 \text{ Hz}$, and (i) $\omega_1^{(3)}=10223.9 \text{ Hz}$

5.2 Natural Frequencies and Mode Shapes. The first nine natural frequencies for the $[0^\circ \text{ Gr-Ep/PZT-5A/PZT-5A}/0^\circ \text{ Gr-Ep}]$ hybrid shell are listed in Table 3. In addition, the plane strain finite element natural frequencies are listed in parentheses next to the analytical results in Table 3. There is good agreement between the analytical and finite element solutions. Since ABAQUS does not have a generalized plane strain element for piezoelectric materials, the out-of-plane modes with displacement in the x direction cannot be captured by the plane strain finite element solution and

are indicated by (---) in Table 3. The corresponding analytically obtained mode shapes are depicted in Fig. 4 by plotting the deformed shapes of material lines that in the reference configuration are parallel to the coordinate axes. Although the shell is assumed to be of infinite width in the x direction, the mode shapes are truncated to a finite width for the purpose of illustration. Three of the lowest nine modes corresponding to $\omega_1^{(2)}$, $\omega_2^{(2)}$, and $\omega_3^{(2)}$ are out-of-plane mode that have non-zero displacement in the x direc-

Table 4 Normalized displacements, stresses and electric potential corresponding to the first nine modes of a hybrid cylindrical shell for $R=0.25 \text{ m}$ and $R/H=5$

Mode	$\frac{u_\theta(0, R+H/2)}{u_\theta(\Theta/(2k), R+H/2)}$	$\frac{u_r(0, R+H/2)}{u_r(\Theta/(2k), R+H/2)}$	$\frac{\sigma_{\theta\theta}(\Theta/(2k), R+H/2)R}{C_\theta u_\theta(\Theta/(2k), R+H/2)}$	$\frac{\sigma_r(\Theta/(2k), R+H/2)R}{C_r u_r(\Theta/(2k), R+H/2)}$	$\frac{\sigma_\theta(0, R+H/4)R}{C_\theta u_\theta(\Theta/(2k), R+H/2)}$	$\frac{\sigma_r(\Theta/(2k), R+H/4)R}{C_r u_r(\Theta/(2k), R+H/2)}$	$\frac{\phi(0, R)e_0}{C_\theta u_\theta(\Theta/(2k), R+H/2)}$
$\omega_1^{(1)}$	49.0339	0.223970	1.79998	-0.00108680	16.6069	-0.0648929	0.00123365
$\omega_2^{(1)}$	3.80600	0.236732	5.96013	-0.00459476	49.7137	-0.191958	0.00496048
$\omega_3^{(1)}$	-2.34905	0.302802	9.56746	-0.00881569	104.211	-0.266612	0.0113607
$\omega_4^{(1)}$	-2.51037	0.166541	12.7747	-0.0129281	79.5715	-0.310141	0.00929069
$\omega_5^{(1)}$	-2.60712	0.137470	15.8511	-0.0166725	84.5251	-0.346370	0.0105779
$\omega_1^{(3)}$	-399.009	-1.89209	56.9388	-0.00918122	317.062	-1.77563	-1.12821

Mode	$\frac{u_x(0, R+H/2)}{u_x(0, R+H/2)}$	$\frac{\sigma_\theta(\Theta/(2k), R+H/2)R}{C_\theta u_\theta(0, R+H/2)}$
$\omega_1^{(2)}$	1	-0.00485243
$\omega_2^{(2)}$	1	-0.0194091
$\omega_3^{(2)}$	1	-0.0436683

Table 5 First nine natural frequencies of a $[-45^\circ \text{ Gr-Ep/PZT-5A/PZT-5A/}45^\circ \text{ Gr-Ep}]$ hybrid cylindrical shell for $R=0.25 \text{ m}$ and $R/H=5$

Mode	Natural Frequency, Hz
$\omega_1^{(1)}$	290.45
$\omega_2^{(1)}$	1431.24
$\omega_3^{(1)}$	3000.98
$\omega_1^{(2)}$	4721.73
$\omega_4^{(1)}$	4777.26
$\omega_1^{(3)}$	6215.21
$\omega_5^{(1)}$	6647.54
$\omega_6^{(1)}$	8558.77
$\omega_2^{(2)}$	8757.78

tion. Five of lowest nine modes, namely $\omega_k^{(1)}$ for $k=1, \dots, 5$, are flexural modes of vibration. The ninth mode $\omega_1^{(3)}$ corresponds to a thickness mode of deformation with significant change in thick-

ness in the radial direction.

Through-the-thickness plots of the displacements and electric potential corresponding to the lowest nine natural frequencies are shown in Figs. 5(a)–5(i) at specific circumferential locations. The variables are plotted after normalization by their respective maximum values. The circumferential displacement u_θ has essentially a linear variation in the radial direction for the fundamental frequency shown in Fig. 5(a). However, u_θ is highly non-linear for the higher modes as evident in Fig. 5(h). The through-the-thickness variation of the stress components $\sigma_{\theta\theta}$, σ_{rr} , $\sigma_{\theta r}$, and $\sigma_{x\theta}$ corresponding to the first nine modes are presented in Fig. 6. The hoop stress $\sigma_{\theta\theta}$ is essentially linear in the thickness direction within each lamina for the fundamental frequency $\omega_1^{(1)}$. For the higher modes, the hoop stress $\sigma_{\theta\theta}$ has a non-linear variation in the graphite-epoxy layers and an essentially linear variation in the piezoelectric layers. The shear stress $\sigma_{\theta x}$ and longitudinal stress $\sigma_{\theta\theta}$ are discontinuous at the interfaces between the graphite-epoxy and piezoelectric laminae due to the abrupt change in material properties. The transverse shear stress $\sigma_{\theta r}$ has an approximately

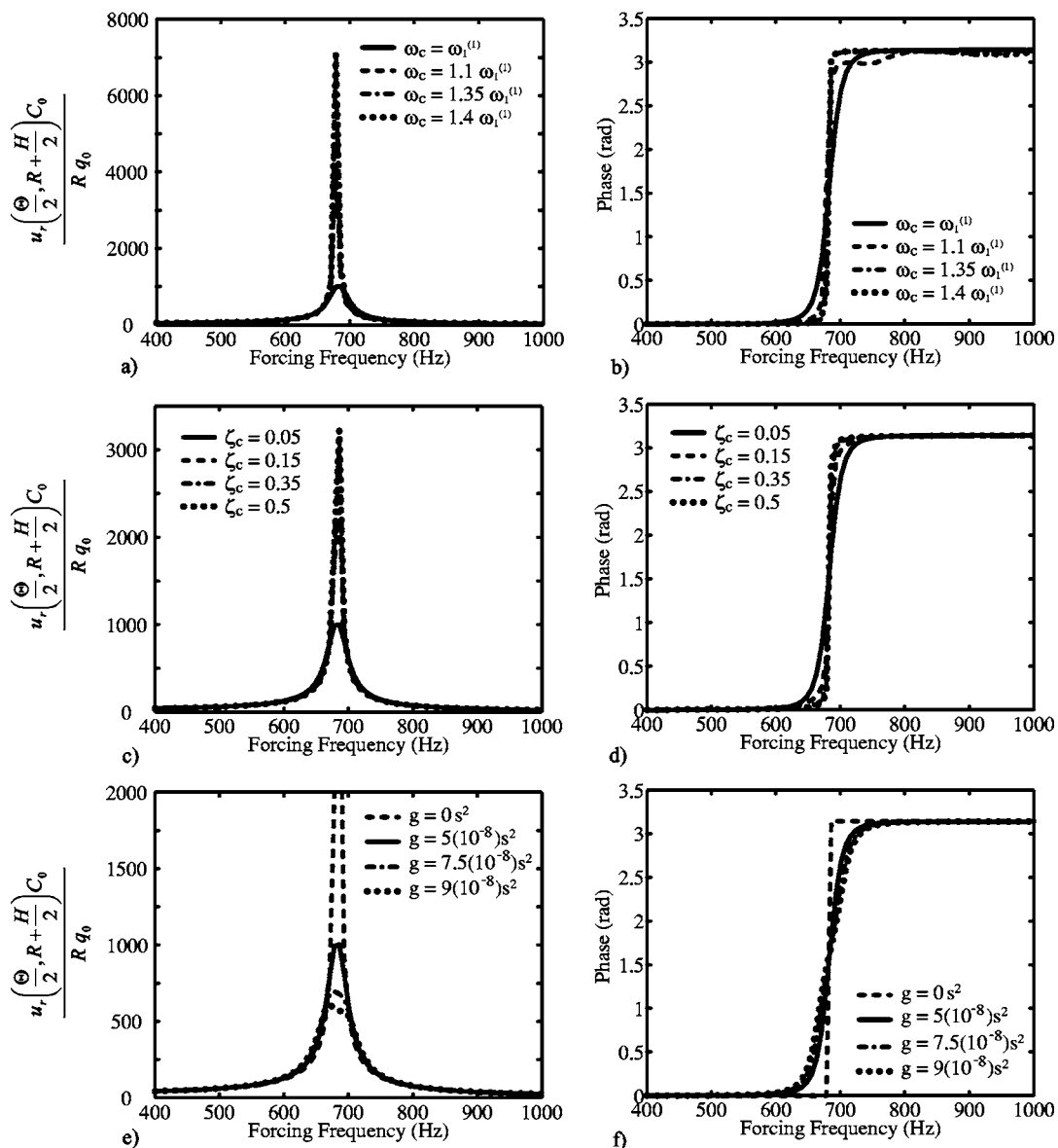


Fig. 7 Magnitude and phase of radial deflection as a function of frequency of a harmonic distributed radial load for a $[0^\circ \text{ Gr-Ep/PZT-5A/PZT-5A/}0^\circ \text{ Gr-Ep}]$ hybrid shell with PPF control, $R=0.25 \text{ m}$, $R/H=5$: (a), (b) $s_c=0.05, g=5(10^{-8}) \text{ s}^2$, (c), (d) $\omega_c=\omega_1^{(1)}, g=5(10^{-8}) \text{ s}^2$, (e), (f) $\omega_c=\omega_1^{(1)}, s_c=0.05$

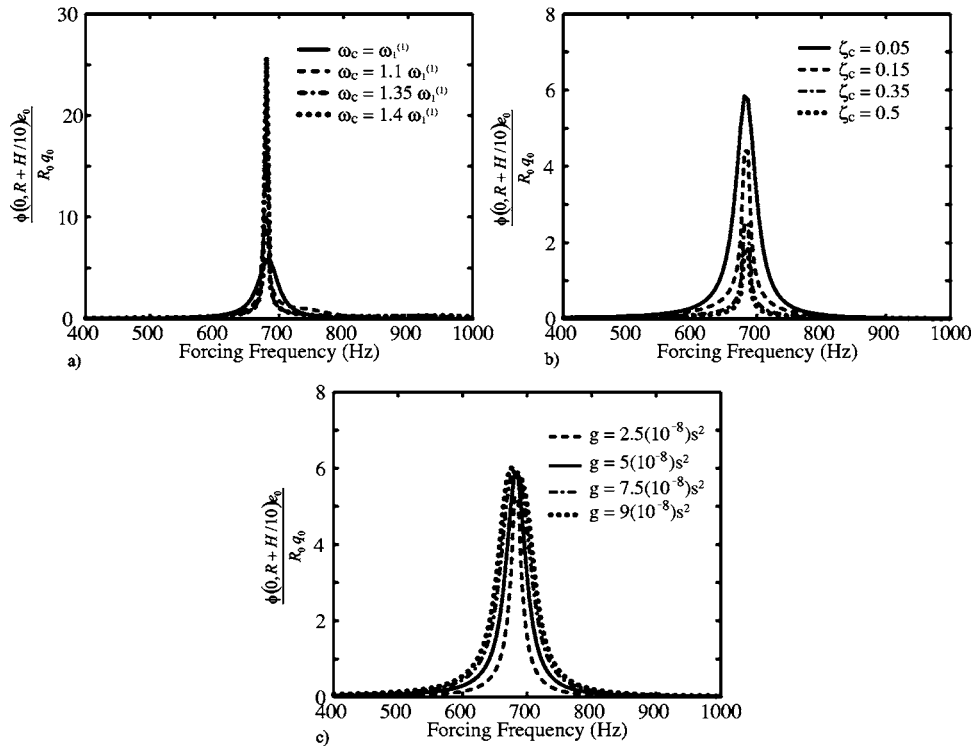


Fig. 8 Magnitude of electric potential to actuator as a function of frequency of a harmonic distributed radial load for a $[0^\circ \text{ Gr-Ep/PZT-5A/PZT-5A}/0^\circ \text{ Gr-Ep}]$ hybrid shell with PPF control, $R=0.25 \text{ m}$, $R/H=5$: (a) $\zeta_c=0.05$, $g=5(10^{-8}) \text{ s}^2$, (b) $\omega_c=\omega_1^{(1)}$, $g=5(10^{-8}) \text{ s}^2$, (c) $\omega_c=\omega_1^{(1)}$, $\zeta_c=0.05$

parabolic variation through the thickness for the flexural modes shown in Figs. 6(a), 6(c), 6(e), 6(g), and 6(h) and a piecewise linear variation for the thickness mode shown in Fig. 6(i). Normalized numerical results for the displacements, stresses, and electric potential are presented in Table 4 for the first nine mode shapes. The natural frequencies of a $[-45^\circ \text{ Gr-Ep/PZT-5A/PZT-5A}/45^\circ \text{ Gr-Ep}]$ composite shell with off-axis fiber-reinforced layers are listed in Table 5.

5.3 Active Damping. Consider the $[0^\circ \text{ Gr-Ep/PZT-5A}/0^\circ \text{ Gr-Ep}]$ hybrid laminate discussed in the previous section of radius $R=0.25 \text{ m}$ and $R/H=5$. It is subjected to the harmonic distributed load (20) on the top surface. A second-order PPF compensator is forced by the potential at a point on the bottom surface of the sensor at $r=r^{(2)}$ and the feedback voltage (24) is applied to the top surface of the PZT-5A shear actuator at $r=r^{(4)}$. Note that $r_s=R-0.1H$ and $n_s=2$ in Eq. (24). We seek to quantify the effectiveness of the piezoelectric shear actuator and the PPF controller for vibration suppression. For a given choice of control parameters ω_c , ζ_c , and g , the steady-state response of the system is computed for a given forcing frequency ω . The magnitude and phase of the radial deflection is plotted as function of the forcing frequency ω for different controller parameters to obtain frequency response curves.

Targeted vibration suppression of the fundamental mode of vibration is achieved by choosing the compensator frequency ω_c to be close to the fundamental frequency $\omega_1^{(1)}=683.292 \text{ Hz}$ (Table 3). Figure 7(a) shows the frequency response curves for controller frequencies of $\omega_c=\omega_1^{(1)}$, $1.1\omega_1^{(1)}$, $1.35\omega_1^{(1)}$, and $1.4\omega_1^{(1)}$. The controller parameters ζ_c and g were kept constant at 0.05 and $5 \times 10^{-8} \text{ s}^2$, respectively, for results in Fig. 7(a). The magnitude of the radial deflection is normalized by the forcing function amplitude q_0 , R , and C_0 , which have values of 1 N/m^2 , 0.25 m , and 21.1 GPa , respectively. The PPF controller reduces the peak radial displacement at resonance. It is observed that the maximum sys-

tem damping is achieved when the controller frequency ω_c is chosen to be equal to the fundamental frequency $\omega_1^{(1)}$. The corresponding phase difference between the radial deflection and the applied harmonic load is shown in Fig. 7(b) as function of the forcing frequency ω . The magnitude and phase frequency response curves for controller damping ratios $\zeta_c=0.05$, 0.15 , 0.35 , and 0.5 are shown in Figs. 7(c) and 7(d) for controller frequency $\omega_c=\omega_1^{(1)}$ and $g=5 \times 10^{-8} \text{ s}^2$. The figure shows a decrease in system damping for increasing controller damping ratio. The response of the system due to changes in the PPF gain parameter g is evident from Fig. 7(e). As the parameter g is increased, the system damping also increases. The magnitude of the electric potential applied to the piezoelectric actuator is shown in Fig. 8 as a function of the forcing frequency for different control parameters. Figure 8(a) demonstrates that the feedback electric potential applied to the piezoelectric actuator is smaller for $\omega_c=\omega_1^{(1)}$ than for $\omega_c=1.4\omega_1^{(1)}$, although the system damping is larger for $\omega_c=\omega_1^{(1)}$ [Fig. 7(a)]. There is no significant change in the feedback potential applied to the parameter is increased [Fig. 8(c)], although the gain parameter has a large effect on the system damping [Fig. 7(e)].

The efficacy of the PPF controller for active vibration suppression of the thickness vibration mode shown in Fig. 4(i) is investigated next. The natural frequency of this thickness mode for $R/H=5$ is $\omega_1^{(3)}=10223.9 \text{ Hz}$. The non-zero circumferential electric field E_θ will influence the transverse normal strain ε_{rr} and the transverse normal stress σ_{rr} through the piezoelectric coefficient e_{13} . Therefore, the feedback controller will introduce active damping in the thickness vibration modes that exhibit significant transverse normal strain ε_{rr} . Figure 9(a) contains the frequency response curves for four different controller frequencies $\omega_c=\omega_1^{(3)}$, $1.1\omega_1^{(3)}$, $1.35\omega_1^{(3)}$, and $1.4\omega_1^{(3)}$. It shows the PPF controller is very effective for the active damping of the thickness mode of vibra-

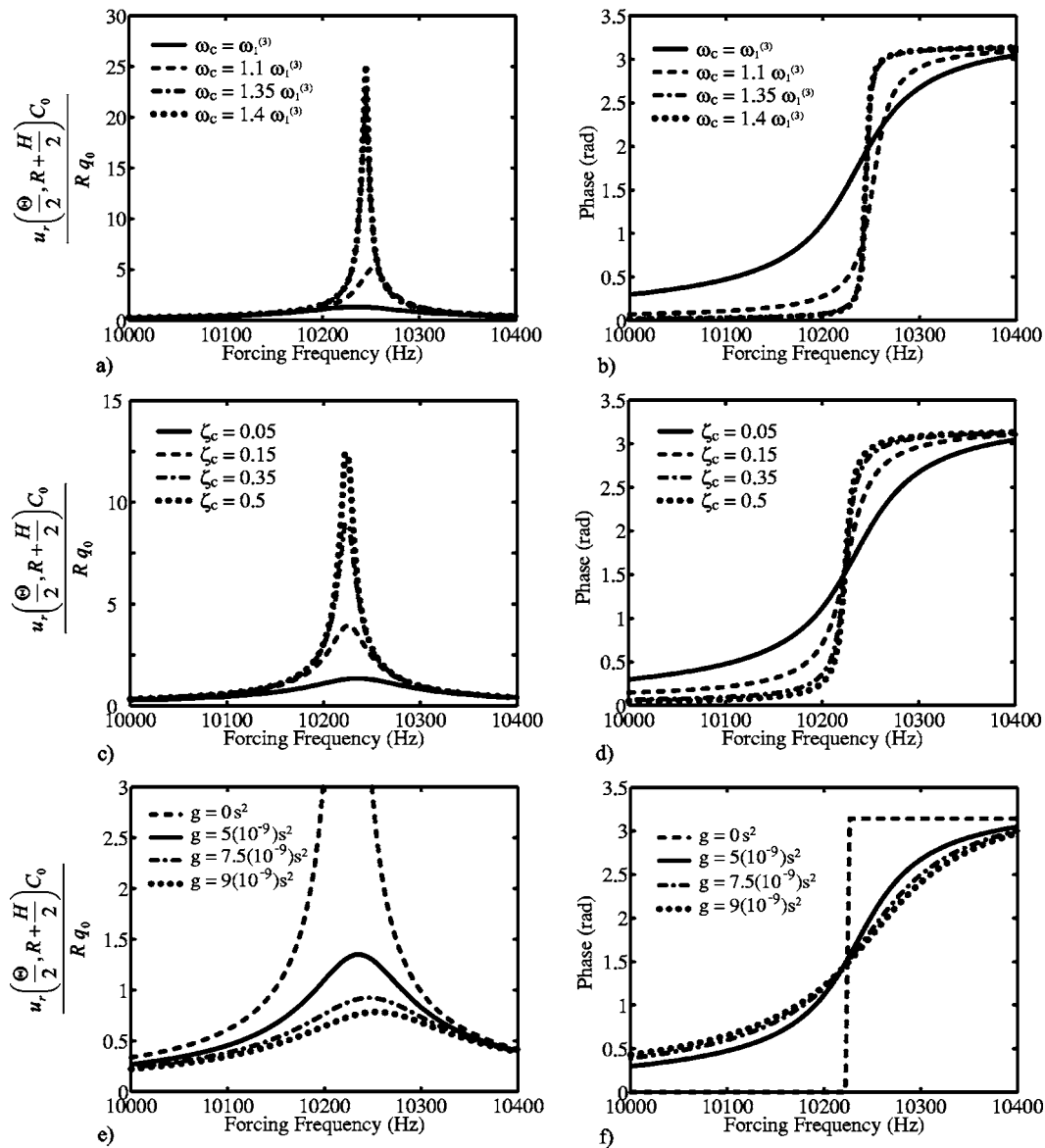


Fig. 9 Magnitude and phase frequency response curves of radial deflection for a harmonic distributed radial load for a $[0^\circ \text{ Gr-Ep/PZT-5A/PZT-5A}/0^\circ \text{ Gr-Ep}]$ hybrid shell with PPF Control, $R=0.25 \text{ m}$, $R/H=5$: (a), (b) $\zeta_c=0.05, g=5(10^{-9}) \text{ s}^2$, (c), (d) $\omega_c=\omega_1^{(3)}, g=5(10^{-9}) \text{ s}^2$, (e), (f) $\omega_c=\omega_1^{(3)}, \zeta_c=0.05$

tion. The largest damping is achieved when the controller frequency ω_c is equal to the natural frequency $\omega_1^{(3)}$. The frequency response curves for various controller damping ratios, depicted in Figs. 9(c) and 9(d), show that a smaller controller damping ratio increases the system damping. As expected, a larger gain parameter g increases the system damping, as shown in Figs. 9(e) and 9(f).

It should be noted that near the resonance frequency, the piezoceramics are expected to behave nonlinearly [34]. However, the results from the present analysis are based on a linear model of the system. The inclusion of nonlinear effects may have a significant effect on the efficacy of the PPF controller and affect the results qualitatively and quantitatively.

6 Conclusions

We have derived an analytical solution for the static deformation, vibration, and active damping of hybrid cylindrical shells with embedded piezoelectric shear sensors and actuators. The edges of the composite shell are simply supported. The governing

equations of linear piezoelectricity, the boundary conditions at the simply supported edges, and the interface conditions between dissimilar layers are exactly satisfied. Suitable displacement and electric potential functions that identically satisfy the boundary conditions are used to reduce the equations that govern the static deformation and steady-state vibrations of a hybrid shell to a set of coupled ordinary differential equations with non-constant coefficients, which are then solved by employing the Frobenius method. The analytical solution thus obtained is valid for any radius-to-thickness ratio.

The analytical and finite element results for the displacements, electric potential, stresses for the static deformation are in good agreement. The first nine natural frequencies, mode shapes, and through-the-thickness plots of the displacements and stresses are presented for hybrid shells consisting of circumferentially poled piezoelectric sensors and actuators sandwiched between two fiber-reinforced composite layers.

Active damping is implemented using a PPF controller. PPF control introduces a second-order compensator which is forced by

the potential from a transverse shear sensor. The controller coordinate, magnified by a gain, is then fed back as a voltage input to a piezoelectric shear actuator. It is found that the PPF controller is effective for active damping of flexural and thickness modes of vibration. Frequency response curves are presented for various controller frequencies, controller damping ratios and feedback gain parameters.

Acknowledgment

The authors gratefully acknowledge the support of the Maine Space Grant Consortium under Collaborative Seed Grant No. EP-02-11.

References

- [1] Fuller, C. R., Elliott, S. J., and Nelson, P. A., 1997, *Active Control of Vibration*, Academic, New York.
- [2] Bailey, T., and Hubbard Jr, J. E., 1985, "Distributed Piezoelectric Polymer Active Vibration Control of a Cantilever Beam," *AIAA J.*, **8**, pp. 605–611.
- [3] Garcia, E., Dosch, J., and Inman, D. J., 1992, "The Application of Smart Structures to the Vibration Suppression Problem," *J. Intell. Mater. Syst. Struct.*, **3**, pp. 659–667.
- [4] Clark, R. L., and Fuller, C. R., 1992, "Experiments on Active Control of Structurally Radiated Sound Using Multiple Piezoelectric Actuators," *J. Acoust. Soc. Am.*, **91**, pp. 3313–3320.
- [5] Crawley, E. F., and Anderson, E. H., 1990, "Detailed Models of Piezoceramic Actuation of Beams," *J. Intell. Mater. Syst. Struct.*, **1**, pp. 4–25.
- [6] Lee, C. K., 1990, "Theory of Laminated Piezoelectric Plates for the Design of Distributed Sensors/Actuators 1. Governing Equations and Reciprocal Relationships," *J. Acoust. Soc. Am.*, **87**, pp. 1144–1158.
- [7] Batra, R. C., Liang, X. Q., and Yang, J. S., 1996, "The Vibration of a Simply Supported Rectangular Elastic Plate due to Piezoelectric Actuators," *Int. J. Solids Struct.*, **33**, pp. 1597–1618.
- [8] Heyliger, P., and Brooks, S., 1995, "Free-vibration of Piezoelectric Laminates in Cylindrical Bending," *Int. J. Solids Struct.*, **32**, pp. 2945–2960.
- [9] Heyliger, P., and Saravanos, D. A., 1995, "Exact Free-vibration Analysis of Laminated Plates with Embedded Piezoelectric Layers," *J. Acoust. Soc. Am.*, **98**, pp. 1547–1557.
- [10] Chen, C.-Q., Shen, Y.-P., and Wang, X.-M., 1996, "Exact Solution of Orthotropic Cylindrical Shell with Piezoelectric Layers under Cylindrical Bending," *Int. J. Solids Struct.*, **33**, 4481–4494.
- [11] Dumir, P. C., Dube, G. P., and Kapuria, S., 1997, "Exact Piezoelectric Solution of Simply-supported Orthotropic Circular Cylindrical Panel in Cylindrical Bending," *Int. J. Solids Struct.*, **34**, pp. 685–702.
- [12] Chen, C.-Q., and Shen, Y.-P., 1998, "Three-dimensional Analysis for the Free Vibration of Finite-length Orthotropic Piezoelectric Circular Cylindrical Shells," *J. Vib. Acoust.*, **120**, pp. 194–198.
- [13] Sun, C. T., and Zhang, X. D., 1995, "Use of Thickness-shear Mode in Adaptive Sandwich Structures," *Smart Mater. Struct.*, **4**, pp. 202–206.
- [14] Electro Ceramic Division, Data for Designers, Morgan Matroc, Bedford, OH.
- [15] Zhang, X. D., and Sun, C. T., 1996, "Formulation of an Adaptive Sandwich Beam," *Smart Mater. Struct.*, **5**, pp. 814–823.
- [16] Zhang, X. D., and Sun, C. T., 1999, "Analysis of a Sandwich Plate Containing a Piezoelectric Core," *Smart Mater. Struct.*, **8**, pp. 31–40.
- [17] Benjeddou, A., Trindade, M. A., and Ohayon, R., 1997, "A Unified Beam Finite Element Model for Extension and Shear Piezoelectric Actuation Mechanisms," *J. Intell. Mater. Syst. Struct.*, **8**, pp. 1012–1025.
- [18] Trindade, M. A., Benjeddou, A., and Ohayon, R., 1999, "Parametric Analysis of the Vibration Control of Sandwich Beams through Shear-based Piezoelectric Actuation," *J. Intell. Mater. Syst. Struct.*, **10**, pp. 377–385.
- [19] Benjeddou, A., and Deü, J.-F., 2002, "A Two-dimensional Closed-form Solution for the Free-vibrations Analysis of Piezoelectric Sandwich Plates," *Int. J. Solids Struct.*, **39**, pp. 1463–1486.
- [20] Vel, S. S., and Batra, R. C., 2001, "Exact Solution for Cylindrical Bending of Laminated Plates with Embedded Shear Actuators," *Smart Mater. Struct.*, **10**, pp. 240–251.
- [21] Vel, S. S., and Batra, R. C., 2001, "Exact Solution for Rectangular Sandwich Plates with Embedded Piezoelectric Shear Actuators," *AIAA J.*, **39**, pp. 1363–1373.
- [22] Benjeddou, A., Gorge, V., and Ohayon, R., 2001, "Use of Piezoelectric Shear Response in Adaptive Sandwich Shells of Revolution 1. Theoretical Formulation," *J. Intell. Mater. Syst. Struct.*, **12**, pp. 235–245.
- [23] Benjeddou, A., Gorge, V., and Ohayon, R., 2001, "Use of Piezoelectric Shear Response in Adaptive Sandwich Shells of Revolution 2. Finite Element Implementation," *J. Intell. Mater. Syst. Struct.*, **12**, pp. 247–257.
- [24] Baillargeon, B., and Vel, S., 2005, "Exact Solution for the Vibration and Active Damping of Composite Plates with Piezoelectric Shear Actuators," *J. Sound Vib.*, **282**, pp. 781–804.
- [25] Goh, C. J., and Caughey, T. K., 1985, "On the Stability Problem Caused by Finite Actuator Dynamics Collected Control of Large Space Structures," *Int. J. Control*, **41**, pp. 787–802.
- [26] Fanson, J. L., and Caughey, T. K., 1990, "Positive Position Feedback for Large Space Structure," *AIAA J.*, **28**, pp. 717–724.
- [27] Friswell, M., and Inman, D. J., 1999, "The Relationship Between Positive Position Feedback and Output Feedback Controllers," *Smart Mater. Struct.*, **8**, pp. 285–291.
- [28] Tiersten, H. F., 1969, *Linear Piezoelectric Plate Vibrations*, Plenum, New York.
- [29] Kreyszig, E., 1999, *Advanced Engineering Mathematics*, Wiley, New York, 8 Ed.
- [30] von Wagner, U., 2003, "Non-linear Longitudinal Vibrations of Piezoceramics Excited by Weak Electric Fields," *Int. J. Non-Linear Mech.*, **38**, pp. 565–574.
- [31] von Wagner, U., 2004, "Non-linear Longitudinal Vibrations of Non-slender Piezoceramic Rods," *Int. J. Non-Linear Mech.*, **39**, pp. 673–688.
- [32] Tang, Y. Y., Noor, A. K., and Xu, K., 1996, "Assessment of Computational Models for Thermoelastoplastic Multilayered Plates," *Comput. Struct.*, **61**, pp. 915–933.
- [33] ABAQUS Users Manual, Version 6.3, Hibbit, Karlsson & Sorensen, Inc., 2002.
- [34] von Wagner, U., and Hagedorn, P., 2003, "Non-linear Effects of Piezoceramics Excited by Weak Electric Fields," *Nonlinear Dyn.*, **31**, pp. 133–149.